# Highly Sensitive Measurement of a Megahertz rf Electric Field with a Rydberg-Atom Sensor

Bang Liu,[1,2] Li-Hua Zhang,[1,2] Zong-Kai Liu,[1,2] Zheng-Yuan Zhang,[1,2] Zhi-Han Zhu,[3] Wei Gao,[3] Guang-Can Guo,[1,2] Dong-Sheng Ding,[1,2,3,*] and Bao-Sen Shi[1,2,†]

[1]*Key Laboratory of Quantum Information, University of Science and Technology of China, Hefei, Anhui 230026, China*

[2]*Synergetic Innovation Center of Quantum Information and Quantum Physics, University of Science and Technology of China, Hefei, Anhui 230026, China*

[3]*Wang Da-Heng Collaborative Innovation Center for Science of Quantum Manipulation and Control, Heilongjiang Province and Harbin University of Science and Technology, Harbin 150080, China*

Rydberg atoms have great potential in electric field measurement and have an advantage with a large frequency bandwidth from the kHz to the THz scale. However, the sensitivity for measuring a weak MHz electric field signal is limited by the spectroscopic resolution, because the weak electric field induces only a small perturbation of the population and energy-level shift of the Rydberg atoms. Here, we report highly sensitive measurement of a weak MHz electric field using electromagnetically induced transparency with Rydberg atoms in a thermal atomic system. Using the heterodyne method on a 30-MHz electric field, we successfully measure the minimum electric field strength to be 37.3 $\mu$V/cm with a sensitivity up to $-65$ dBm/Hz and a linear dynamic range over 65 dB. Additionally, we measure an amplitude-modulated signal and demodulate the signal with a fidelity over 98%. This work extends the sensitivity of atomic sensors for measuring MHz electric fields, which advances atomic electric field-sensing technology.

## I. INTRODUCTION

Rydberg atoms have been widely used for electric field measurement owing to their large electric dipole moments and polarizabilities [1]. Their various energy levels, covering ranges from the kHz to the THz scale, make it easier to expand their operating bands than those of conventional antennas without changing the sensing device, so Rydberg atoms show great potential for measuring electric fields. Initially, Rydberg atoms were detected with ionization pulses, but those were destructive [2]. Then, the use of electromagnetically induced transparency (EIT) with Rydberg atoms [3,4] was proposed as a direct, nondestructive method to probe Rydberg energy levels. Using the Rydberg-EIT method, researchers have studied the spectra of Rydberg atoms modulated by rf electric fields and obtained the strengths of the applied rf electric fields [5,6]. Electric-field-measurement techniques based on Rydberg atoms have progressed from weak to strong fields and successfully measured field strengths from the nV/m [6–8] to the kV/m scale [9,10]. Furthermore, an electric field with a large frequency bandwidth can be measured from below 1 kHz [11] to tens of GHz [12–14]. All these efforts are aimed at establishing an electric field measurement with an atomic standard.

Researchers are also applying Rydberg atomic measurements of electric fields to areas such as rf polarization [15], subwavelength imaging [16,17], and digital communications [18–20]. This is especially significant for technologies involving approximately MHz electric fields such as shortwave international and regional broadcasting and aviation air-to-ground communications, because of the long wavelengths and long propagation distances of these fields. However, the Chu limit of conventional antennas [21] restricts the channel capacity when the antenna is much smaller than the wavelength of the electromagnetic wave. In contrast, a sensor based on Rydberg atoms is not limited by size, the vapor cell used is generally a few cm long, and the data capacity of the sensor far exceeds that of a conventional antenna of the same size [22]. Therefore, it makes sense to develop a technique that measures a MHz electric field with high sensitivity using Rydberg atoms.

Although electric fields can be measured over a wide range of frequencies based on Rydberg atoms, it is rare to measure a weak MHz signal. It is difficult to measure the shift of an EIT spectrum because the weak field causes very small perturbations to the energy level, making

---

*dds@ustc.edu.cn
†drshi@ustc.edu.cn

the EIT spectrum change very little. Some groups have studied related problems [9,23,24], but they were more focused on strong fields. In a strong field, the Rydberg atomic energy levels have a large Stark shift, which leads to mixing of many different energy levels. Floquet theory is used to calculate the Rydberg-EIT spectrum of a strong field. Information on the applied electric field can be extracted by comparing the calculated Rydberg-EIT spectrum of the field with the experimentally measured spectrum. Researchers have used this method to measure strong fields with amplitudes greater than 5 kV/m [10], but it is difficult to measure a weak electric field with the method because the minimum measurable field strength is only 0.1 V/m.

In this study, we focus on the highly sensitive measurement of a MHz rf electric field using a hot vapor cell. The outside electric field can be coupled directly to the atoms without the need for additional devices. As the MHz electric field does not couple any transitions between two Rydberg levels in our experiment, we use the ac Stark shift to measure the MHz electric field. And we use the heterodyne technique [6,25] to amplify the system response to a weak signal electric field by applying a local electric field. We achieve measurement of a 30-MHz electric field with a sensitivity of −65 dBm/Hz and dynamic range of 65 dB. In addition, we demonstrate measurement of an amplitude-modulated (AM) 1-kHz signal electric field based on Rydberg atoms with a fidelity over 98%. Our work helps applications of Rydberg atomic sensors such as long-distance communication, over-the-horizon radar, and rf identification (RFID).

## II. EXPERIMENT SETUP

Figure 1(a) is the energy-level diagram of a cesium (Cs) atom, where $|1\rangle$ is the ground state, $|2\rangle$ and $|3\rangle$ are two low-lying excited states, and $|4\rangle$ is the Rydberg state of the Cs atom. The experimental setup is depicted in Fig. 1(b). The probe light passes through a 7-cm vapor cell in parallel with the reference light, and the dressing light and the coupling light propagate backwards from the probe light. The probe light is focused into a cell ($1/e^2$-waist radius of approximately 200 $\mu$m) and couples the ground state $|1\rangle = |6S_{1/2}, F = 4\rangle$ to the intermediate state $|2\rangle = |6P_{3/2}, F = 5\rangle$ with Rabi frequency $\Omega_p$. The dressing light is focused into the cell ($1/e^2$-waist radius of approximately 500 $\mu$m) and couples the two intermediate states $|2\rangle = |6P_{3/2}, F = 5\rangle$ and $|3\rangle = |7S_{1/2}, F = 4\rangle$ with Rabi frequency $\Omega_d$. The coupling light ($1/e^2$-waist radius of approximately 500 $\mu$m) drives the transition from $|3\rangle = |7S_{1/2}, F = 4\rangle$ to the Rydberg state $|4\rangle = |55P_{3/2}\rangle$ with detuning $\Delta_c$ and Rabi frequency $\Omega_c \sim 2\pi \times 4$ MHz. A four-energy-level structure is used here to avoid the use of lasers below 580 nm, thus avoiding the ionization shielding effect of Cs atoms in the atomic vapor cell due to photoelectric ionization [26–28]. In the three-photon EIT scheme, lasers are simple commercial lasers, which can be acquired easily and we do not require complex frequency-doubling lasers, which are very expensive. We use two rf signal sources to generate the rf wave, one as the local oscillator (LO) and the other as the signal, where the LO has a small detuning from the signal. The signal and LO electric field pass through a transmission line through an
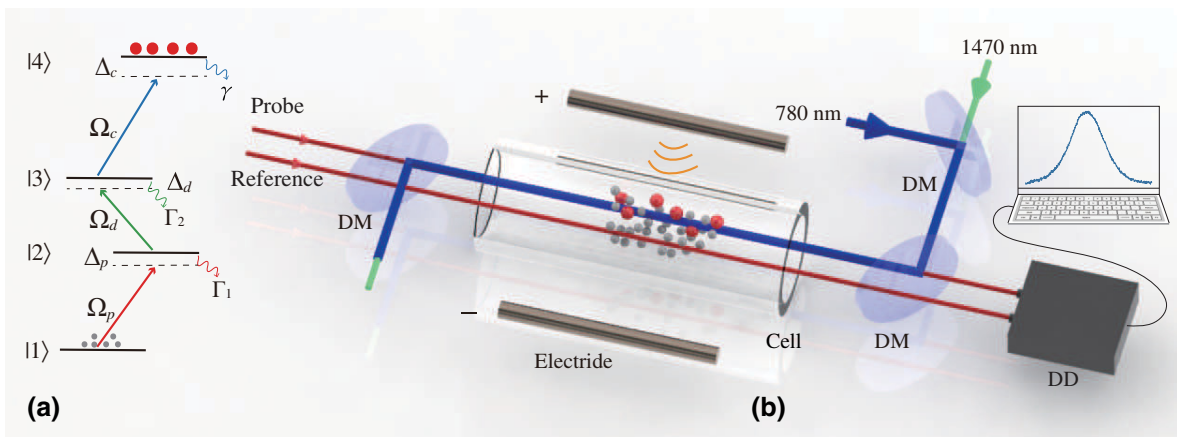


FIG. 1. (a) Ladder-type four-level atomic energy diagram consisting of a ground state $|1\rangle$, two low-lying excited states $|2\rangle$ and $|3\rangle$, and a Rydberg state $|4\rangle$. An 852-nm probe light drives the transition $|1\rangle = |6S_{1/2}, F = 4\rangle \rightarrow |2\rangle = |6P_{3/2}, F = 5\rangle$, a 1470-nm dressing light couples the transition $|2\rangle = |6P_{3/2}, F = 5\rangle \rightarrow |3\rangle = |7S_{1/2}, F = 4\rangle$, and a 780-nm coupling light drives the transition $|3\rangle = |7S_{1/2}, F = 4\rangle \rightarrow |4\rangle = |55P_{3/2}\rangle$ of cesium atoms. (b) Overview of the experimental setup. The probe light and the reference light propagate in parallel through a Cs vapor cell. The probe light (red) overlaps the counterpropagating coupling light (blue) and dressing light (green) to form an EIT configuration. The transmission difference between the probe and reference lights is detected by a differencing photodetector. Two electrode rods are placed parallel to each other on both sides of the vapor cell 4 cm apart. Labels: DM, dichroic mirror; DD, differencing photodetector.

rf power splitter to the electrode rods. The transmission of the probe and reference lights is detected by a balanced photodetector.

## III. RESULTS AND DISCUSSION

First, we experimentally study the three-photon EIT in the Cs vapor cell involving the Rydberg state [29]. We fix the frequencies of the probe light and the dressing light such that each resonated with the corresponding transitions. Figure 2(a) shows the EIT spectrum of the Cs atoms obtained by scanning the detuning $\Delta_c$ of the coupling light.

When $\Delta_c = 0$, the spectrum exhibits a narrow transmission window, which is a typical EIT feature. To model our system, we consider the four-level system in Fig. 1(a). The detunings of the probe light, dressing light, and coupling light are denoted as $\Delta_p$, $\Delta_d$, and $\Delta_c$, respectively; and $\Gamma_1$, $\Gamma_2$, and $\gamma$ are the corresponding decay rates of the atomic states $|2\rangle$, $|3\rangle$, and $|4\rangle$, respectively. Using the rotating-wave approximation, the Hamiltonian of the system in the interaction picture can be written as

$$H_I = \hbar\Delta_p\sigma_{22} + \hbar\left(\Delta_p + \Delta_d\right)\sigma_{33} + \hbar\left(\Delta_p + \Delta_d + \Delta_c\right)\sigma_{44}$$
$$- \hbar/2\left(\Omega_p\sigma_{12} + \Omega_d\sigma_{23} + \Omega_c\sigma_{34} + \text{H.c.}\right), \quad (1)$$

where $\sigma_{ij} = |i\rangle\langle j|$ $(i,j = 1,2,3,4)$ are the atomic transition operators. Considering spontaneous radiation, the system satisfies the Lindblad equation

$$\dot{\rho} = -\frac{i}{\hbar}[H,\rho] + \mathcal{L}(\Gamma_{21}) + \mathcal{L}(\Gamma_{32}) + \mathcal{L}(\Gamma_{43}), \quad (2)$$

where $\rho$ is the density matrix of the system, and $\mathcal{L}(\Gamma_{ij}) = \Gamma_{ij}/2\left(2\sigma_{ji}\rho\sigma_{ij} - \sigma_{ii}\rho - \rho\sigma_{ii}\right)$ is the Lindblad operator with $\Gamma_{21} = \Gamma_1$, $\Gamma_{32} = \Gamma_2$, and $\Gamma_{43} = \gamma$. Considering the Doppler effect due to the thermal motion of the atoms, we correct the detunings to $\Delta_p = \Delta_p - k_p v$, $\Delta_d = \Delta_d + k_d v$,

and $\Delta_c = \Delta_c + k_c v$, where $k_p$, $k_d$, and $k_c$ are the corresponding wave vectors, and $v$ denotes the atom velocity. The steady-state solution of the system density matrix can be obtained by solving Eq. (2). The susceptibility

$$\chi_{21} = -\int \frac{2N(v)|d_{21}|^2}{\hbar\epsilon_0\Omega_p}\rho_{21}(v)\,dv \quad (3)$$

is further obtained, where $N(v) = N_0/u\sqrt{\pi}\exp\left(-v^2/u^2\right)$, $u = (2k_B T/M)^{-1/2}$ is the most probable speed, $N_0$ is the atomic density, $d_{21}$ is the transition dipole matrix element between $|2\rangle$ and $|1\rangle$, $k_B$ is the Boltzmann constant, $T$ is the temperature of the cell, and $M$ is the mass of a Cs atom. The absorption coefficient can be calculated using the imaginary part of the susceptibility, $\alpha = k_p\text{Im}(\chi_{21})$. The transmission is calculated as $\exp(-\alpha l)$ and plotted as a function of coupling detuning $\Delta_c$ in Fig. 2(a), where $l$ is the length of the cell. The probe-light transmission obtained by solving the master equation (red) agrees well with the experiment (gray).

We then investigate the effect of an rf electric field on the atomic EIT spectrum. In the experiment, only one signal source is turned on, and its frequency is set to 30 MHz with an output power of 8 dBm. The rf electric field signal is applied to the electrode rods along the transmission line. Turning on the rf electric field caused the entire EIT spectrum to shift to the left, and the spectrum is shifted by about 17 MHz, as shown in Fig. 2(b). This can be explained by the ac Stark shift [1,30] $\delta = -(1/2)\alpha E^2$, where $\alpha$ is the polarizability and $E$ the amplitude of the electric field. The Rydberg state is more sensitive to the external electric field owing to the higher polarizability, which induces a large energy shift. The ground and intermediate states produce a small energy shift because of the lower polarizability, so we can ignore it. When considering the perturbation of the Rydberg state by the external electric field, the detuning of coupling light in Eq. (1) is updated to $\Delta_c = \Delta_c + \delta$.
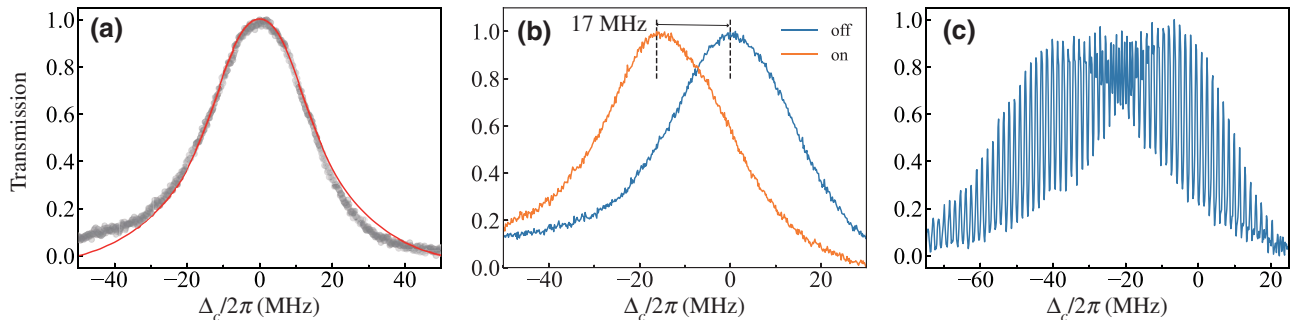


FIG. 2. (a) Three-photon EIT spectrum of Cs atoms. The gray dots are the experimental data, and the red line is the theoretical result. (b) EIT spectrum in an external rf electric field. The rf electric field causes the EIT spectrum to shift to the left. The blue is the spectrum when the rf electric field is turned off, and the orange correspond to the spectrum when the rf electric field is turned on and $P = 8$ dBm. (c) EIT spectrum of the Cs atoms when two electric fields are applied, where $f_{\text{sig}} = 30$ MHz and $f_{\text{LO}} = 30.05$ MHz. The EIT spectrum is modulated with $\Delta\omega = 50$ kHz by the beat signals of the two electric fields. The transmission in the pictures is normalized.

The EIT spectrum obviously shifts to the left as $\delta < 0$. Using the ac Stark effect, we can calibrate the magnitude of the electric field inside the vapor cell. With the Alkali Rydberg Calculator (ARC) package [31], we can calculate the polarizability of the Rydberg atoms to be 2500.68 MHz cm$^2$/V$^2$, and we can obtain the electric field as 167 mV/cm at a Stark shift of 17 MHz. The electric field felt by the atoms is significantly smaller compared to the measured voltage between the electrode rods, due to the shielding effect of the vapor cell. Note that the condition we consider is different from the resonant situation in Ref. [5], which leads to the Autler-Townes (AT) splitting [32]. Because the applied rf electric field is far from resonance, it does not couple the Rydberg state transition. The electric field just causes an ac Stark shift of the Rydberg energy level, which leads to a shift of the EIT resonance peak.

Next, we demonstrate measurement of a weak MHz rf electric field based on Rydberg atoms through applying a LO electric field using a heterodyne method, which is our main work. As mentioned above, the MHz rf electric field can cause an energy shift of the Rydberg state, and further shift the EIT spectrum of the cesium atoms. When two electric fields with different frequencies are applied, each perturbs the Rydberg energy level differently, so the EIT spectrum takes on an alternative character. We turn on two signal sources and set their frequencies to 30 and 30.05 MHz, respectively; the EIT spectrum is shown in Fig. 2(c). First, the EIT spectrum is clearly modulated, and the measured modulation frequency is exactly equal to the difference between the LO and signal electric field. In addition, the EIT spectrum is shifted to the left. The total electric field is $\mathbf{E}_{LO} + \mathbf{E}_{sig}$, and the Stark shift caused by the electric field is

$$\delta = -\frac{1}{2}\alpha\left(\mathbf{E}_{LO} + \mathbf{E}_{sig}\right)^2. \tag{4}$$

Here we set the LO to be phase synchronized with the signal in our experiment, so we let $\phi_{LO} = \phi_{sig}$, where $\Delta\omega$ represents the detuning of the LO and signal. When Eq. (4) is expanded, there are some fast-varying terms. By averaging over time, we get

$$\bar{\delta} = \bar{\delta}_0 - \frac{1}{2}\alpha\left[E_{LO}E_{sig}\cos(\Delta\omega * t)\right], \tag{5}$$

where $\bar{\delta}_0 = -1/4\alpha\left(E_{LO}^2 + E_{sig}^2\right)$ is the average ac Stark shift caused by the LO and signal electric field.

The energy shift is modulated by the beat frequency in Eq. (5), so we can see the beat-frequency signal in the EIT spectrum. Additionally, information on the magnitude of the signal electric field can be extracted by measuring the beat-frequency components of the probe light. In the experiment, the output of the two signal sources is applied

to the electrode rods after the rf power splitter. The LO frequency is set to 30.05 MHz and the signal frequency to 30 MHz, and the LO power is $P_{LO} = 7$ dBm. The coupling light is fixed at an optimal operating point, and the change in probe-light intensity with time is monitored through the digital oscilloscope. Then, we use the spectrum analyzer to measure the intensity of the beat signal. The beat-signal intensity is shown in Fig. 3(a) for different signal electric field strengths. The intensity of the received beat signal is approximately proportional to the strength of the applied signal electric field, as described by Eq. (5). We achieve a dynamic range of 65 dB for measuring a 30-MHz rf electric field, and the power sensitivity is up to $-65$ dBm/Hz. Using the previous calibration relationship between the electric field in the electrode rods and the input power, which we obtain in Fig. 2(b), we calculate the sensitivity for the electric field strength to be 37.3 $\mu$V/cm/Hz$^{1/2}$. The instantaneous bandwidth of the system is shown in Fig. 3(b). The instantaneous bandwidth of the system $B$
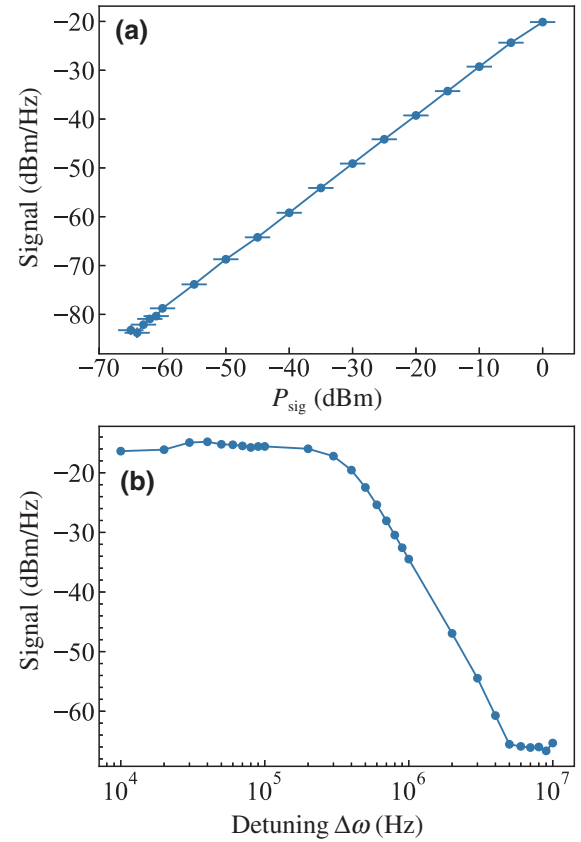


FIG. 3. (a) Dynamic range of the system with $P_{LO} = 7$ dBm and $\Delta\omega = 50$ kHz. The beat signal strength shows a linear relationship with input power in a range of 65 dB. (b) Instantaneous bandwidth of the system with $P_{LO} = 7$ dBm and $P_{sig} = 0$ dBm. As the detuning of the signal electric field and the local-oscillator electric field increases, the beat signal strength keeps decreasing. Considering the negative detuning, we get a 3-dB bandwidth of 0.8 MHz.
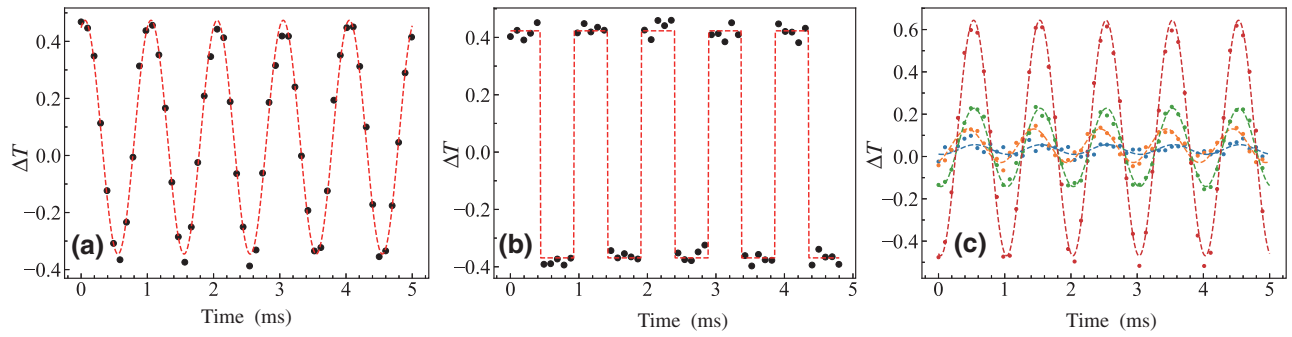
FIG. 4. Results of demodulation of a 30-MHz carrier wave. (a),(b) Signals obtained by demodulating the carrier with sinusoidal modulation and square-wave modulation, respectively, with a modulation frequency of 1 kHz. The signal is well restored with 98% fidelity for both sinusoidal and square-wave modulations. The black dots represent the signal after demodulation using Rydberg atoms, and the red dashed line is the modulated signal. (c) Signals obtained by Rydberg atomic demodulation at different modulation depths, 2% (blue), 5% (green), 10% (orange), 30% (red).

reaches 0.8 MHz considering the negative detuning of the signal with the LO. The bandwidth of the system mainly depends on the probe photon scattering rate of the intermediate atomic resonance (of order 10 MHz) [33]. Here we define a parameter $\eta = B/\omega_c$, i.e., the ratio of bandwidth and carrier frequency, to measure the relative bandwidth. Compared with Ref. [6], the parameter in our case is much larger than theirs. As they use GHz electric field to couple the Rydberg levels resonantly. Once the frequency of the signal deviates too much from the frequency of the LO, the response of the Rydberg atoms to the signal will be weaker. However, here we use the ac Stark shift, which is a nonresonant effect, and atoms can respond to the electric field with a lager bandwidth.

We demonstrate short-wave communication using Rydberg atoms based on measurement of a MHz electric field using Rydberg atoms. rf electric fields can be used to carry information through sound signals and transmit information over great distances using the propagation properties of the carrier wave. Experimentally, we use a signal source to generate a 30-MHz rf electric field and apply amplitude modulation to it with a frequency of 1 kHz [34–36]. The modulation depth is 30% and the carrier power is 7 dBm. The transmission of the probe light is recorded by the digital oscilloscope when the coupling light is locked at the optimal operating point. As shown in Fig. 4, the modulation information is better extracted for both sinusoidal and square-wave modulations. We use $A \sin(\omega t + \varphi) + B$ to perform the fit where $\omega = 2\pi \times 1$ kHz and then calculate the deviation to obtain the fidelity, mainly to measure the degree of signal distortion after atomic demodulation. Compared to modulated signal, the fidelity of the demodulated signal reaches 98%. Experimentally at different modulation depths, we extract modulated signals from the spectra as shown in the Fig. 4(c). Obviously, we can see that as the modulation depth increases, the clearer the extracted signal is. The Rydberg atom acts as a demodulator without the need for complex electronic

demodulation devices. The modulation signal is carried directly in the transmission of the probe light, and we need only to record it using the photoelectric detector. The carrier band we are concerned with is the MHz range. Although its signal bandwidth has a limit, this is not a major issue in areas such as broadcasting. Actually, broadcasting is generally for long-distance transmission, and most of the information transmitted is sound signals, which are mostly in kHz, and the instantaneous bandwidth we obtain in the experiment is 0.8 MHz, which is sufficient for transmitting sound information. We are more concerned about the effect of the sensor size. When entering the electrically small regime [22], the efficiency of conventional antennas is greatly reduced while Rydberg atom-based sensors are not affected.

## IV. CONCLUSION

In conclusion, we investigate the perturbation of the Rydberg energy level by a MHz electric field, and realize measurement of a weak electric field signal using the heterodyne method. We achieve measurement of a 30-MHz electric field with a 65-dB dynamic range and a sensitivity reaching −65 dBm/Hz. On this basis, we demonstrate the recovery of an AM signal with 98% fidelity. We improve the performance of the Rydberg atom sensor in measuring electric fields in the MHz band, which will facilitate implementation of a wide-band Rydberg atom receiver. Measurements of electric fields at lower frequencies are also being explored [11], although many difficulties are encountered. It will be beneficial to use Rydberg atoms in more situations such as long-wave radar and submarine communication.

[1] T. F. Gallagher, *Rydberg Atoms* (Cambridge University Press, New York, 1994).

[2] A. Osterwalder and F. Merkt, Using High Rydberg States as Electric Field Sensors, Phys. Rev. Lett. **82,** 1831 (1999).

[3] A. Mohapatra, T. Jackson, and C. Adams, Coherent Optical Detection of Highly Excited Rydberg States using Electromagnetically Induced Transparency, Phys. Rev. Lett. **98,** 113003 (2007).

[4] H. Kübler, J. Shaffer, T. Baluktsian, R. Löw, and T. Pfau, Coherent excitation of Rydberg atoms in micrometre-sized atomic vapour cells, Nat. Photonics **4,** 112 (2010).

[5] J. A. Sedlacek, A. Schwettmann, H. Kübler, R. Löw, T. Pfau, and J. P. Shaffer, Microwave electrometry with Rydberg atoms in a vapour cell using bright atomic resonances, Nat. Phys. **8,** 819 (2012).

[6] M. Jing, Y. Hu, J. Ma, H. Zhang, L. Zhang, L. Xiao, and S. Jia, Atomic superheterodyne receiver based on microwave-dressed Rydberg spectroscopy, Nat. Phys. **16,** 911 (2020).

[7] J. A. Gordon, M. T. Simons, A. H. Haddab, and C. L. Holloway, Weak electric-field detection with sub-1 Hz resolution at radio frequencies using a Rydberg atom-based mixer, AIP Adv. **9,** 045030 (2019).

[8] S. Kumar, H. Fan, H. Kübler, A. J. Jahangiri, and J. P. Shaffer, Rydberg-atom based radio-frequency electrometry using frequency modulation spectroscopy in room temperature vapor cells, Opt. Express **25,** 8625 (2017).

[9] D. A. Anderson, S. A. Miller, G. Raithel, J. Gordon, M. Butler, and C. Holloway, Optical Measurements of Strong Microwave Fields with Rydberg Atoms in a Vapor Cell, Phys. Rev. Appl. **5,** 034003 (2016).

[10] E. Paradis, G. Raithel, and D. A. Anderson, Atomic measurements of high-intensity VHF-band radio-frequency fields with a Rydberg vapor-cell detector, Phys. Rev. A **100,** 013420 (2019).

[11] Y.-Y. Jau and T. Carter, Vapor-Cell-Based Atomic Electrometry for Detection Frequencies below 1 kHz, Phys. Rev. Appl. **13,** 054034 (2020).

[12] L. A. Downes, A. R. MacKellar, D. J. Whiting, C. Bourgenot, C. S. Adams, and K. J. Weatherill, Full-Field Terahertz Imaging at Kilohertz Frame Rates using Atomic Vapor, Phys. Rev. X **10,** 011027 (2020).

[13] J. A. Gordon, C. L. Holloway, A. Schwarzkopf, D. A. Anderson, S. Miller, N. Thaicharoen, and G. Raithel, Millimeter wave detection via Autler-Townes splitting in rubidium Rydberg atoms, Appl. Phys. Lett. **105,** 024104 (2014).

[14] C. G. Wade, N. Šibalić, N. R. de Melo, J. M. Kondo, C. S. Adams, and K. J. Weatherill, Real-time near-field terahertz imaging with atomic optical fluorescence, Nat. Photonics **11,** 40 (2017).

[15] J. Sedlacek, A. Schwettmann, H. Kübler, and J. Shaffer, Atom-Based Vector Microwave Electrometry using Rubidium Rydberg Atoms in a Vapor Cell, Phys. Rev. Lett. **111,** 063001 (2013).

[16] C. L. Holloway, J. A. Gordon, A. Schwarzkopf, D. A. Anderson, S. A. Miller, N. Thaicharoen, and G. Raithel, Sub-wavelength imaging and field mapping via electromagnetically induced transparency and Autler-Townes splitting in Rydberg atoms, Appl. Phys. Lett. **104,** 244102 (2014).

[17] C. L. Holloway, M. T. Simons, J. A. Gordon, P. F. Wilson, C. M. Cooke, D. A. Anderson, and G. Raithel, Atom-based RF electric field metrology: From self-calibrated measurements to subwavelength and near-field imaging, IEEE Trans. Electromagn. Compat. **59,** 717 (2017).

[18] D. H. Meyer, K. C. Cox, F. K. Fatemi, and P. D. Kunz, Digital communication with Rydberg atoms and amplitude-modulated microwave fields, Appl. Phys. Lett. **112,** 211108 (2018).

[19] Z. Song, H. Liu, X. Liu, W. Zhang, H. Zou, J. Zhang, and J. Qu, Rydberg-atom-based digital communication using a continuously tunable radio-frequency carrier, Opt. Express **27,** 8848 (2019).

[20] Z.-K. Liu, L.-H. Zhang, B. Liu, Z.-Y. Zhang, G.-C. Guo, D.-S. Ding, and B.-S. Shi, Deep learning enhanced Rydberg multifrequency microwave recognition, Nat. Commun. **13,** 1 (2022).

[21] L. J. Chu, Physical limitations of omni-directional antennas, J. Appl. Phys. **19,** 1163 (1948).

[22] K. C. Cox, D. H. Meyer, F. K. Fatemi, and P. D. Kunz, Quantum-Limited Atomic Receiver in the Electrically Small Regime, Phys. Rev. Lett. **121,** 110502 (2018).

[23] Y. Jiao, X. Han, Z. Yang, J. Li, G. Raithel, J. Zhao, and S. Jia, Spectroscopy of cesium Rydberg atoms in strong radio-frequency fields, Phys. Rev. A **94,** 023832 (2016).

[24] S. A. Miller, D. A. Anderson, and G. Raithel, Radio-frequency-modulated Rydberg states in a vapor cell, New J. Phys. **18,** 053017 (2016).

[25] D. H. Meyer, P. D. Kunz, and K. C. Cox, Waveguide-Coupled Rydberg Spectrum Analyzer from 0 to 20 GHz, Phys. Rev. Appl. **15,** 014053 (2021).

[26] M. G. Bason, M. Tanasittikosol, A. Sargsyan, A. Mohapatra, D. Sarkisyan, R. Potvliege, and C. Adams, Enhanced electric field sensitivity of rf-dressed Rydberg dark states, New J. Phys. **12,** 065015 (2010).

[27] M. Viteau, J. Radogostowicz, M. Bason, N. Malossi, D. Ciampini, O. Morsch, and E. Arimondo, Rydberg spectroscopy of a Rb MOT in the presence of applied or ion created electric fields, Opt. Express **19,** 6007 (2011).

[28] J. Xu, A. Gozzini, F. Mango, G. Alzetta, and R. Bernheim, Photoatomic effect: Light-induced ejection of Na and Na$_2$ from polydimethylsiloxane surfaces, Phys. Rev. A **54,** 3146 (1996).

[29] N. Thaicharoen, K. Moore, D. Anderson, R. Powel, E. Peterson, and G. Raithel, Electromagnetically induced transparency, absorption, and microwave-field sensing in a Rb vapor cell with a three-color all-infrared laser system, Phys. Rev. A **100,** 063427 (2019).

[30] N. B. Delone and V. P. Krainov, AC Stark shift of atomic energy levels, Phys.-Usp. **42**, 669 (1999).

[31] N. Šibalić, J. Pritchard, C. Adams, and K. Weatherill, ARC: An open-source library for calculating properties of alkali Rydberg atoms, Comput. Phys. Commun. **220**, 319 (2017).

[32] S. H. Autler and C. H. Townes, Stark effect in rapidly varying fields, Phys. Rev. **100**, 703 (1955).

[33] D. H. Meyer, Z. A. Castillo, K. C. Cox, and P. D. Kunz, Assessment of Rydberg atoms for wideband electric field sensing, J. Phys. B **53**, 034001 (2020).

[34] D. A. Anderson, R. E. Sapiro, and G. Raithel, An atomic receiver for AM and FM radio communication, IEEE Trans. Antennas Propag. **69**, 2455 (2020).

[35] C. L. Holloway, M. T. Simons, A. H. Haddab, C. J. Williams, and M. W. Holloway, A real-time guitar recording using Rydberg atoms and electromagnetically induced transparency: Quantum physics meets music, AIP Adv. **9**, 065110 (2019).

[36] Y. Jiao, X. Han, J. Fan, G. Raithel, J. Zhao, and S. Jia, Atom-based receiver for amplitude-modulated baseband signals in high-frequency radio communication, Appl. Phys. Express **12**, 126002 (2019).